NANO LETTERS
Cite This: Nano Lett. 2018, 18, 805−810
Letter
pubs.acs.org/NanoLett

Surface Photovoltage Measurements on a Particle Tandem Photocatalyst for Overall Water Splitting

Mauricio A. Melo, Jr.,[†,‡] Zongkai Wu,[†] Benjamin A. Nail,[†] Alexandra T. De Denko,[†] Ana F. Nogueira,[‡] and Frank E. Osterloh*[,†]

[†]Department of Chemistry, University of California, Davis, One Shields Avenue, Davis, California 95616, United States
[‡]Institute of Chemistry, University of Campinas, UNICAMP, P.O. Box 6154, Campinas, São Paulo 13084-971, Brazil

Supporting Information

ABSTRACT: Surface photovoltage spectroscopy (SPS) is used to measure the photopotential across a Ru−$SrTiO_3$:Rh/$BiVO_4$ particle tandem overall water splitting photocatalyst. The tandem is synthesized from Ru-modified $SrTiO_3$:Rh nanocrystals and $BiVO_4$ microcrystals by electrostatic assembly followed by thermal annealing. It splits water into H_2 and O_2 with an apparent quantum efficiency of 1.29% at 435 nm and a solar to hydrogen conversion efficiency of 0.028%. According to SPS, a photovoltage develops above 2.20 eV, the effective band gap of the tandem, and reaches its maximal value of −2.45 V at 435 nm (2.44 mW cm^{-2}), which corresponds to 96% of the theoretical limit of the photocatalyst film on the fluorine-doped tin-oxide-coated glass (FTO) substrate. Charge separation is 82% reversible with 18% of charge carriers being trapped in defect states. The unusually strong light intensity dependence of the photovoltage (1.16 V per decade) is attributed to depletion layer changes inside of the $BiVO_4$ microcrystals. These findings promote the understanding of solar energy conversion with inorganic particle photocatalysts.

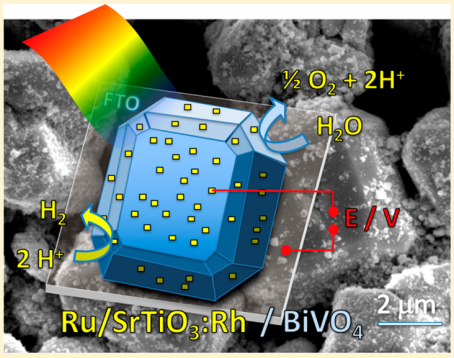

KEYWORDS: *Photovoltage, overall water splitting, Z-scheme, surface photovoltage spectroscopy*

Because of the total integration of light absorbing and electrocatalytic components, particle-based photocatalysts for overall water splitting (OWS)[1−4] can be over 1 order of magnitude less expensive than photoelectrochemical or photovoltaic cells for fuel production.[1,5,6] While "first generation" OWS catalysts operate on the basis of a single absorber configuration,[7−14] "second generation" tandem or Z-scheme photocatalysts[2,15−24] employ the dual absorber configuration, where two separate light absorbers are connected in series, either via a solid interface or via a liquid interface using redox couples as mediators. The theoretical limiting efficiency of such systems has been calculated as high as 28%;[9,10,25] however, existing tandems achieve no more than 1.1%,[26] which can be attributed to surface recombination of charge carriers, ineffective charge separation, and the H_2/O_2 back-reaction.[27] Overall, photochemical charge separation is not well-understood for OWS catalysts because there are no good methods available to probe the charge distribution inside of particles. Photoelectrochemical measurements on particle films are convoluted by large charge transport resistances,[28−31] and transient absorption studies on suspended particles[32,33] do not provide any information on the photovoltage, which determines the electrical power output of the photocatalysts. Here we circumvent these problems by using surface photovoltage spectroscopy (SPS) to probe the photovoltage of a photocatalyst film. In SPS, the contact potential difference (CPD) of a sample film on top of a conductive substrate is recorded with a contactless Kelvin probe as a function of the incident photon energy.[34−36] The change of the CPD under illumination corresponds to a photovoltage that develops across the sample film. The sign of the photovoltage is determined by the majority carrier type; e.g., electrons moving to the back of the film yield a negative voltage (Figure S1).[37] The size of the photovoltage is limited by the band offsets in the film and provides information about the ability of the photocatalyst to separate charge carriers under illumination.[38−40] The onset energy of the photovoltage equals the effective bandgap of the sample.[41] In this way, SPS provides information about parameters that are central to the operation of water splitting photocatalysts.

The Ru−$SrTiO_3$:Rh/$BiVO_4$ direct contact tandem catalyst for this study was assembled electrostatically in aqueous solution at pH 3.5 following the protocol reported by Kudo and co-workers (details in the Supporting Information).[17] The synthesis was completed by thermal annealing at 300 °C for 60−90 min under argon gas, followed by mild ultrasonication in acidified water to remove excess Ru−$SrTiO_3$:Rh nanoparticles. SEM images of the product (Figure 1) reveal the presence of $BiVO_4$ microparticles decorated with Ru−

Received: September 18, 2017
Revised: December 11, 2017
Published: December 25, 2017

DOI: 10.1021/acs.nanolett.7b04020
Nano Lett. 2018, 18, 805−810

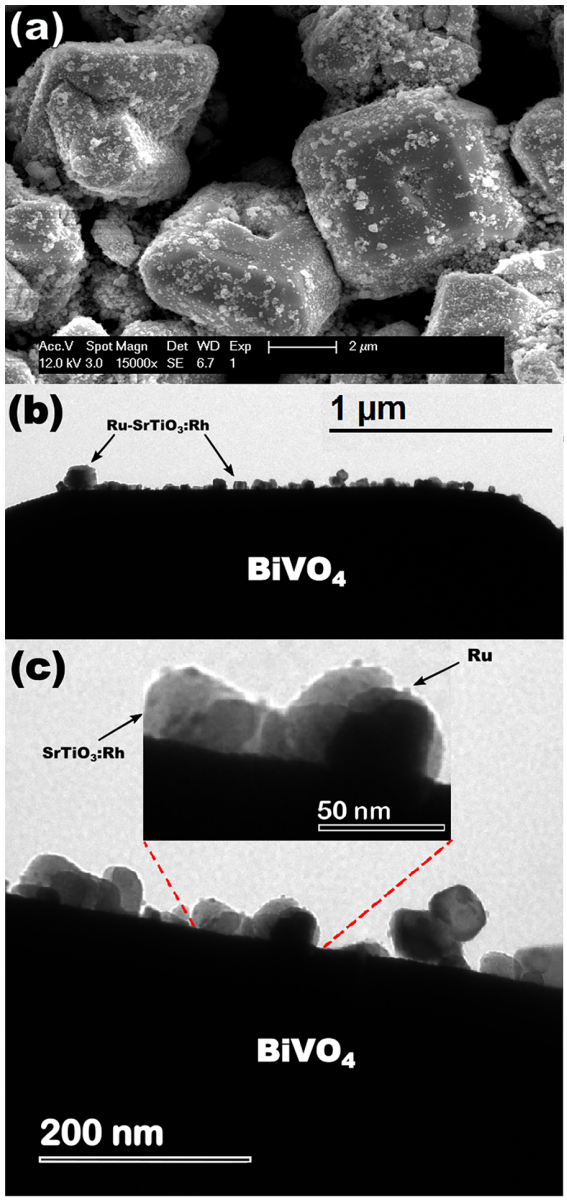

Figure 1. (a) SEM and (b, c) TEM images of the direct contact composite synthesized by annealing the components at 300 °C for 60 min. Individual $SrTiO_3$:Rh and Ru particles can be clearly observed.

$SrTiO_3$:Rh nanocrystals on their surface. Based on inductively coupled plasma optical emission spectroscopy (ICP-OES), the $BiVO_4$/Ru−$SrTiO_3$:Rh weight ratio is 3.5/1, and powder XRD data shows that the tandem only contains phases of the building blocks (Figure S2).

According to UV−vis diffuse reflectance spectra (Figure 2) the particle tandem maintains the optical properties of the components. The absorption onset at 530 nm is between that of $BiVO_4$ (516 nm) and Ru−$SrTiO_3$:Rh (532 nm). The absence of an absorption peak at 700 nm (for Rh^{4+}) confirms that Rh is in the Rh^{3+} oxidation state.[42] Additional absorption in the range 530−800 nm is from the Ru-nanoparticle cocatalyst.

Figure 2b shows hydrogen and oxygen evolution (2:1 mol ratio) from water at pH 3.5, when the tandem is illuminated with visible light (>400 nm). After 7 h, 122.5 μmol of H_2 and

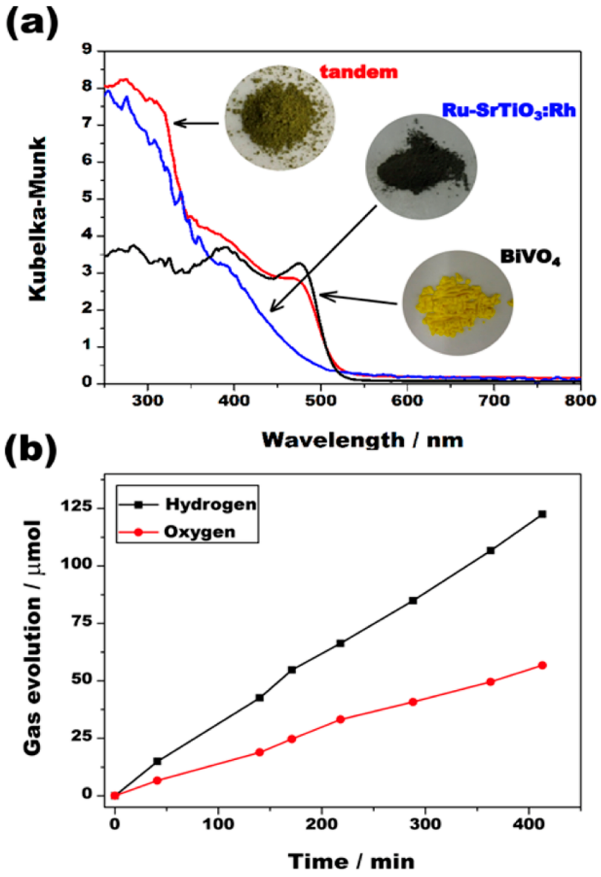

Figure 2. (a) UV−vis diffuse reflectance spectra of the separate light absorbers and the tandem (after heating at 300 °C for 90 min). (b) Visible-light-driven production of hydrogen (■) and oxygen (●) of the composite annealed at 300 °C for 90 min. Conditions: 51.5 mg of catalyst in 50 mL of H_2SO_4 aqueous solution at pH 3.5. Light power: 1098 mW cm^{-2}, >400 nm (aq $NaNO_2$ long-pass filter).

56.7 μmol of O_2 are produced, which corresponds to 17.8 μmol H_2 h^{-1}. The apparent quantum efficiency (AQE) is 1.29% at 435 nm (0.445 W cm^{-2}, 2.54 cm^2 illuminated area, H_2 data in Figure S3), and the solar to hydrogen (STH) conversion efficiency was determined as 0.028% (Figure S4). This performance is comparable to other Ru−$SrTiO_3$:Rh/$BiVO_4$ tandems (Table S1), but below the system reported in 2016, which owes its higher performance to Mo-doping of the $BiVO_4$ and La-codoping of $SrTiO_3$:Rh.[26]

To obtain insight into the ability of the nano- and microscale absorbers to generate and separate photochemical charge carriers, surface photovoltage spectroscopy (SPS) measurements were performed on thin films of the tandem and on its components. The spectra are shown in Figure 3a, and an energy scheme showing charge transfer paths and maximum theoretical photovoltage $V_{th,max}$ values at the interfaces is given in Figure 3b. All samples generate a negative photovoltage under illumination that can be attributed to the transfer of photoelectrons (majority carrier) into the fluorine-doped tin-oxide-coated glass (FTO, see also Figure S1),[40] while photoholes are trapped in the tandem film.

For the $SrTiO_3$:Rh nanocrystal film, the photovoltage onset occurs at 2.04 eV, and the maximum voltage of −0.99 V is observed at 2.65 eV. According to Figure 3b, the maximum theoretical photovoltage $V_{th,max}$ for the FTO/$SrTiO_3$:Rh

DOI: 10.1021/acs.nanolett.7b04020
Nano Lett. 2018, 18, 805−810

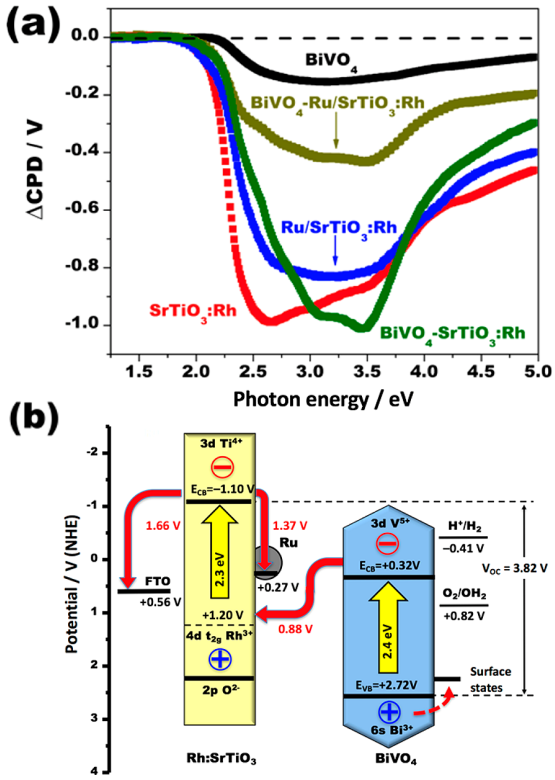

Figure 3. (a) Surface photovoltage spectroscopy (SPS) data for $BiVO_4$, $SrTiO_3$:Rh, Ru−$SrTiO_3$:Rh, and Ru−$SrTiO_3$:Rh/$BiVO_4$ sample films on fluorine-doped tin-oxide-coated glass (FTO) substrates under vacuum. ΔCPD is the contact potential difference change relative to the dark. Above 4.0 eV the photovoltage is limited by the vanishing light intensity of the Xe lamp (see Figure S5). (b) Energy diagram of the tandem catalyst on top of the FTO substrate at neutral pH = 7. pH 7 is chosen as reference point because it is close to the point of zero charge for many metal oxides and because neutral water is often employed in photocatalytic water splitting experiments. Values for the band edges and work function for FTO were taken from the literature.[38,39] Red arrows indicate electron−hole transfer. Numerical values at the arrows correspond to the maximum *theoretical* photovoltage $V_{th,max}$ at each interface, as defined by the band edges/Fermi levels of the donor and acceptor, respectively.

contact is $[E_F(FTO) - E_{CB}(SrTiO_3:Rh)] = -1.66$ V. This maximum theoretical photovoltage corresponds to the thermodynamic driving force for electrons to move across the FTO/$SrTiO_3$:Rh contact based on the Fermi level, E_F, of the acceptor and the conduction band edge, E_{CB}, of the donor.[39] The experimental photovoltage only reaches 60% of this limit because of the low light intensity (0.1−0.25 mW cm^{-2}, see Figure S5) under the SPS measurement conditions. After modification of $SrTiO_3$:Rh with 1 wt % Ru nanoparticles, the photovoltage of the particle film is decreased to −0.82 V (at 3.00 eV). This reduction indicates that photoelectrons inject into the cocatalyst (E_F = +0.27 V vs NHE) instead of the FTO substrate. Electron transfer from $SrTiO_3$:Rh to Ru would be expected because the Ru nanoparticles function as proton reduction cocatalyst. For a $BiVO_4$ particle film, the photovoltage onset is observed at 2.20 eV, and the maximum (−0.15 V) occurs at 3.20 eV. This voltage corresponds to 63% of the maximum theoretical photovoltage $[E_F(FTO) - E_{CB}(BiVO_4)]$ = +0.56 V − 0.32 V = 0.24 V.[38,43] The SPS spectrum for a film of the assembled particle tandem is shown as the olive-green trace in Figure 3a. It shows a photo-onset of 2.20 eV and a voltage maximum of −0.40 V at 3.0 eV, nearly twice the $BiVO_4$ only value. In the 3.0−3.5 eV illumination interval, the voltage stays constant, and then it declines due to the diminishing intensity of the light source (see Figure S5). The resemblance of the spectrum to that of $BiVO_4$ and its higher photovoltage suggest that the photochemical charge generation in the tandem is due to excitation of Ru−$SrTiO_3$:Rh and $BiVO_4$ light absorbers in series, as shown in Figure 3b. To rule out the possibility of both absorbers acting separately, SPS spectra for physical mixtures of Ru−$SrTiO_3$:Rh and $BiVO_4$ were also recorded. As can be seen in Figure S6, mixtures of the tandem components produce a voltage spike at 2.49 eV that stems from independent excitation of Ru−$SrTiO_3$:Rh to FTO. This spike is absent in the spectra of the tandem, suggesting that both absorbers are electrically connected in series. Here, $BiVO_4$ generates electrons that inject into $SrTiO_3$:Rh and from there into the Ru particles or into the FTO substrate.

The observation of directional electron transfer across the particle films is remarkable considering that the tandem particles have a random orientation on the FTO substrate (Figure S7). Selective injection of electrons into the FTO substrate is possible, however, if photoholes become trapped in the $BiVO_4$ particles. This is shown in the equivalent circuit diagram in Figure S8. Hole trapping at the $BiVO_4$ particles prevents recombination with the mobile photoelectrons, which can move to the FTO substrate by diffusion. Adding up theoretical voltage contributions from the FTO/$SrTiO_3$:Rh interface (−1.66 V) and the $SrTiO_3$:Rh/$BiVO_4$ contact (−0.88 V), one obtains −1.66 − 0.88 V = −2.54 V as maximum theoretical photovoltage $V_{th,max}$ for the configuration shown in Figure 3b. The observed voltage (−0.40 V at 3.0 eV) is only 16% of this value. This discrepancy can be attributed to the low light intensity of the measurement (0.25 mW cm^{-2}) and to trapping of electrons at the Ru particle, as discussed for Ru−$SrTiO_3$:Rh above. To test the electron trapping hypothesis, a Ru-nanoparticle tandem was assembled also from $BiVO_4$ and $SrTiO_3$:Rh components. The SPS spectrum of this Ru-free configuration (Figure 3a) resembles that of Ru−$SrTiO_3$:Rh/$BiVO_4$ tandem. Its photovoltage of —0.94 V (at 3.0 eV) is over two times the previous value, confirming that the Ru particles act as electron traps.

Next, to evaluate the intensity dependence, photovoltage values for the Ru-free tandem film were recorded under variable intensity (0.007−2.440 mW cm^{-2}) and fixed wavelength (2.85 eV) illumination (Figure 4a). When the light is turned on, a negative voltage develops, which takes approximately 850 s to reach a steady state. The slow time scale of the photovoltage suggests that electron transport in the particle film is due to diffusion.[38] As can be seen in Figure 4b, higher illumination intensity causes the steady state photovoltage values to increase monotonically. Saturation of the photovoltage at −2.45 V occurs when the illumination intensity reaches 2.44 mW cm^{-2}. This voltage is 96% of the theoretical maximum photovoltage predicted in Figure 3b for the FTO/$SrTiO_3$:Rh/$BiVO_4$ configuration. This confirms that both of the two light absorbers act in tandem and donate electrons at a Fermi energy equal to the conduction band of each absorber. Based on the reversibility of the photovoltage scan (insert of Figure 4b), most of the photoholes are trapped in shallow traps while some carriers become trapped in deep traps, likely at the $BiVO_4$ surface. This deep trap charge population can be estimated as 18% of the total separated charge, based on the residual

DOI: 10.1021/acs.nanolett.7b04020
Nano Lett. 2018, 18, 805−810

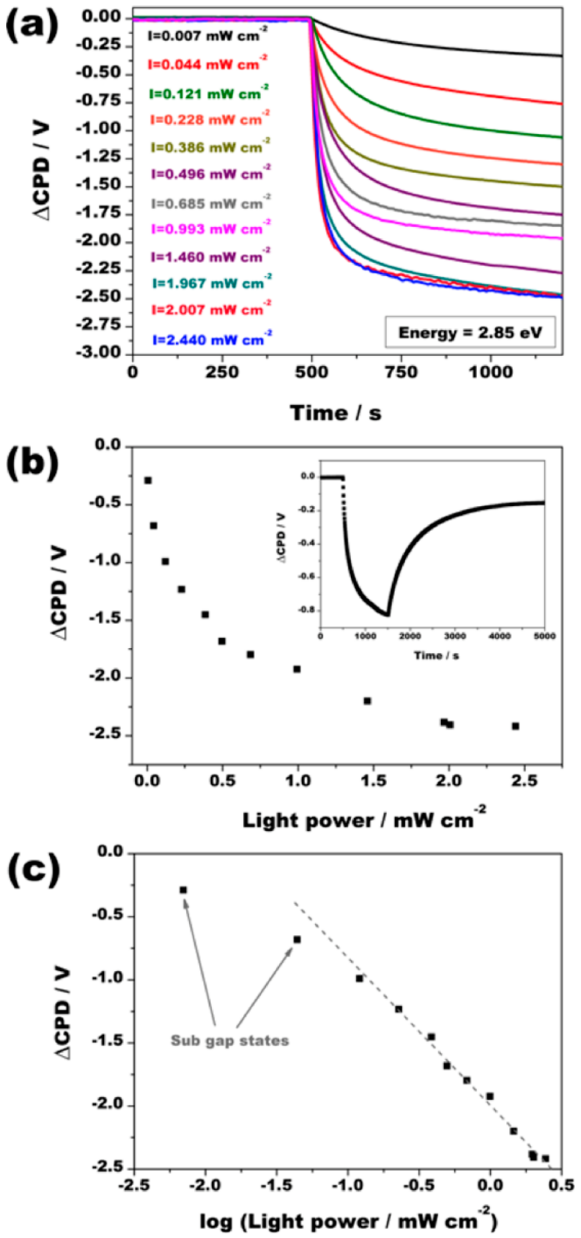

Figure 4. (a) Variable light intensity photovoltage at 2.85 eV fixed photon energy. The time constant τ for reaching 63% of the full photovoltage is ~530 s. (b) Plot of photovoltage versus light power. Inset: baseline recovery after light on cycle (2.85 eV light at 0.106 mW cm^{-2}). After 3500 s, a voltage of −0.152 V remains (18% of maximum). (c) Plot of photovoltage versus logarithm of light power. Deviations at low illumination power are attributed to excitation of subdefect states in the tandem.

photovoltage that remains 3500 s after turning off the light. Under working conditions of the tandem, these holes would oxidize water, thereby increasing the maximum possible photovoltage of the tandem to the open circuit voltage value V_{OC} given by the energy difference between the conduction band edge of $SrTiO_3$:Rh and the valence band edge of $BiVO_4$ (Figure 3b). SPS cannot probe this contribution to the photovoltage because there is no liquid electrolyte present in the particle film under the vacuum conditions of the experiment.

A replot of the data in Figure 4c reveals a logarithmic dependence of the photovoltage on illumination power (Figure 4c) for nearly the entire intensity range. (The deviation at low illumination power is attributed to excitation of subgap states in $BiVO_4$.[44]) It is interesting to compare this logarithmic trend to the behavior of a photovoltaic junction. According to the Shockley diode equation the open circuit voltage of single photovoltaic junction increases by 59 mV with every 10-fold increase of illumination power.[45−47] For a dual junction (tandem), one would then expect a 118 mV photovoltage increase per decade. In contrast, the slope for the tandem is −1.16 V per decade, which is 10 times larger than the theory predicts. This deviation is attributed to the increasing depletion of the tandem system under the conditions of the SPS experiment. When the illumination intensity is low, the tandem film is electrically neutral, and the bands inside of the light absorbers are flat. Under these conditions most photogenerated charge carriers are lost to Shockley Read Hall recombination at mid gap states at the particle surfaces.[48,49] Charge separation in the tandem film improves as the light intensity increases, and the film becomes depleted of majority carriers. A depletion layer can then form inside of the $BiVO_4$ particles (Figure S9), which keeps majority carriers away from detrimental surface states. This reduces electron−hole recombination and causes the logarithmic increase of the photovoltage in Figure 4c. This depletion model explains not only the low quantum efficiency of the tandem (1.29% at 435 nm), but also the nonideal behavior of other water splitting photocatalysts, where the quantum efficiency is found to improve at higher illumination intensity.[50−52] The need for a depletion layer to suppress electron−hole recombination is also well-documented for $BiVO_4$[53−57] and for Fe_2O_3 photoanodes.[58−60] It is the reason why a 0.4−1.0 V voltage bias is generally required to turn on water oxidation with these materials.

In conclusion, we have used surface photovoltage spectroscopy for the first time to measure the photovoltage that develops across a tandem particle photocatalyst under illumination. Photochemical charge separation begins at 2.20 eV, the effective bandgap of the tandem, and reaches its maximum at 3.0 eV, where both absorbers show strong light absorption. Electrons are found to be majority carriers, and charge transport occurs by diffusion. Charge separation in the tandem is 82% reversible and increases with light intensity. Under 2.44 mW cm^{-2} (2.85 eV) illumination, the tandem generates a maximum photovoltage of −2.45 V, which corresponds to 96% of the theoretical limit of the FTO/$SrTiO_3$:Rh/$BiVO_4$ sample configuration, based on the energetics of the semiconductors. This shows that both light absorbers act in tandem and generate electrons at a Fermi energy equal to the conduction band of each absorber. Because no liquid water is present, photoholes are trapped in the $BiVO_4$ particles which become increasingly depleted of majority carriers. This explains the abnormally strong photovoltage increase with light intensity (−1.16 V per decade of intensity increase). These findings provide new insight into the factors that control electron−hole separation in particle-based photocatalysts and into the role of light intensity to improve photovoltage and photocatalytic activity.

DOI: 10.1021/acs.nanolett.7b04020
Nano Lett. 2018, 18, 805−810

■ ASSOCIATED CONTENT

Supporting Information

The Supporting Information is available free of charge on the ACS Publications website at DOI: 10.1021/acs.nanolett.7b04020.

Experimental details, instrument setup, XRD patterns, gas evolution data, Xe emission spectrum, catalyst comparison, SPS data, band diagrams, and an equivalent circuit diagram (PDF)

■ AUTHOR INFORMATION

Corresponding Author

*E-mail: fosterloh@ucdavis.edu. Phone: +1 530 754 6242.

ORCID

Ana F. Nogueira: 0000-0002-0838-7962

Frank E. Osterloh: 0000-0002-9288-3407

Notes

The authors declare no competing financial interest.

■ ACKNOWLEDGMENTS

We gratefully acknowledge São Paulo Research Foundation (FAPESP—Grant 2014/22388-3) for financial support and fellowship, the National Science Foundation (NSF Grant 1464938), and the U.S. Department of Energy, Office of Science, Office of Basic Energy Sciences under Award Number DE-SC0015329.

■ REFERENCES

(1) Fabian, D. M.; Hu, S.; Singh, N.; Houle, F. A.; Hisatomi, T.; Domen, K.; Osterloh, F. E.; Ardo, S. *Energy Environ. Sci.* **2015**, *8*, 2825−2850.

(2) Kudo, A. *MRS Bull.* **2011**, *36*, 32−38.

(3) Maeda, K.; Teramura, K.; Saito, N.; Inoue, Y.; Kobayashi, H.; Domen, K. *Pure Appl. Chem.* **2006**, *78*, 2267−2276.

(4) Hisatomi, T.; Kubota, J.; Domen, K. *Chem. Soc. Rev.* **2014**, *43*, 7520−7535.

(5) Pinaud, B. A.; Benck, J. D.; Seitz, L. C.; Forman, A. J.; Chen, Z. B.; Deutsch, T. G.; James, B. D.; Baum, K. N.; Baum, G. N.; Ardo, S.; Wang, H. L.; Miller, E.; Jaramillo, T. F. *Energy Environ. Sci.* **2013**, *6*, 1983−2002.

(6) James, B. D.; Baum, G. N.; Perez, J.; Baum, K. N. *Technoeconomic Analysis of Photoelectrochemical (PEC) Hydrogen Production*; Technical Report for the Department of Energy on Contract GS-10F-009J: Arlington, VA, 2009; http://www1.eere.energy.gov/hydrogenandfuelcells/pdfs/pec_technoeconomic_analysis.pdf.

(7) Nozik, A. J. *Appl. Phys. Lett.* **1977**, *30*, 567−569.

(8) Walter, M. G.; Warren, E. L.; McKone, J. R.; Boettcher, S. W.; Mi, Q. X.; Santori, E. A.; Lewis, N. S. *Chem. Rev.* **2010**, *110*, 6446−6473.

(9) Bolton, J. R.; Strickler, S. J.; Connolly, J. S. *Nature* **1985**, *316*, 495−500.

(10) Varghese, O. K.; Grimes, C. A. *Sol. Energy Mater. Sol. Cells* **2008**, *92*, 374−384.

(11) Kato, H.; Asakura, K.; Kudo, A. *J. Am. Chem. Soc.* **2003**, *125*, 3082−3089.

(12) Ohno, T.; Bai, L.; Hisatomi, T.; Maeda, K.; Domen, K. *J. Am. Chem. Soc.* **2012**, *134*, 8254−8259.

(13) Maeda, K.; Teramura, K.; Lu, D. L.; Takata, T.; Saito, N.; Inoue, Y.; Domen, K. *J. Phys. Chem. B* **2006**, *110*, 13753−13758.

(14) Maeda, K.; Teramura, K.; Lu, D. L.; Takata, T.; Saito, N.; Inoue, Y.; Domen, K. *Nature* **2006**, *440*, 295−295.

(15) Sayama, K.; Yoshida, R.; Kusama, H.; Okabe, K.; Abe, Y.; Arakawa, H. *Chem. Phys. Lett.* **1997**, *277*, 387−391.

(16) Abe, R.; Takata, T.; Sugihara, H.; Domen, K. *Chem. Commun.* **2005**, 3829−3831.

(17) Sasaki, Y.; Nemoto, H.; Saito, K.; Kudo, A. *J. Phys. Chem. C* **2009**, *113*, 17536−17542.

(18) Abe, R. *J. Photochem. Photobiol., C* **2010**, *11*, 179−209.

(19) Maeda, K.; Higashi, M.; Lu, D. L.; Abe, R.; Domen, K. *J. Am. Chem. Soc.* **2010**, *132*, 5858−5868.

(20) Maeda, K. *ACS Catal.* **2013**, *3*, 1486−1503.

(21) Chen, S.; Qi, Y.; Hisatomi, T.; Ding, Q.; Asai, T.; Li, Z.; Ma, S. S. K.; Zhang, F.; Domen, K.; Li, C. *Angew. Chem., Int. Ed.* **2015**, *54*, 8498.

(22) Sayama, K.; Mukasa, K.; Abe, R.; Abe, Y.; Arakawa, H. *Chem. Commun.* **2001**, 2416−2417.

(23) Moniz, S. J. A.; Shevlin, S. A.; Martin, D. J.; Guo, Z.-X.; Tang, J. *Energy Environ. Sci.* **2015**, *8*, 731.

(24) Zhou, P.; Yu, J. G.; Jaroniec, M. *Adv. Mater.* **2014**, *26*, 4920−4935.

(25) Bard, A. J. *J. Photochem.* **1979**, *10*, 59−75.

(26) Wang, Q.; Hisatomi, T.; Jia, Q.; Tokudome, H.; Zhong, M.; Wang, C.; Pan, Z.; Takata, T.; Nakabayashi, M.; Shibata, N.; Li, Y.; Sharp, I. D.; Kudo, A.; Yamada, T.; Domen, K. *Nat. Mater.* **2016**, *15*, 611−615.

(27) Osterloh, F. E. *J. Phys. Chem. Lett.* **2014**, *5*, 2510−2511.

(28) Osterloh, F. E. *Top. Curr. Chem.* **2015**, *371*, 105−142.

(29) Osterloh, F. E. *Chem. Soc. Rev.* **2013**, *42*, 2294−2320.

(30) Iwashina, K.; Kudo, A. *J. Am. Chem. Soc.* **2011**, *133*, 13272−13275.

(31) Jia, Q.; Iwashina, K.; Kudo, A. *Proc. Natl. Acad. Sci. U. S. A.* **2012**, *109*, 11564−11569.

(32) Robel, I.; Kuno, M.; Kamat, P. V. *J. Am. Chem. Soc.* **2007**, *129*, 4136−4137.

(33) Ben-Shahar, Y.; Scotognella, F.; Waiskopf, N.; Kriegel, I.; Dal Conte, S.; Cerullo, G.; Banin, U. *Small* **2015**, *11*, 462−471.

(34) Kronik, L.; Shapira, Y. *Surf. Sci. Rep.* **1999**, *37*, 1−206.

(35) Dittrich, T.; Fiechter, S.; Thomas, A. *Appl. Phys. Lett.* **2011**, *99*, 084105-1−084105-3.

(36) Gross, D.; Mora-Sero, I.; Dittrich, T.; Belaidi, A.; Mauser, C.; Houtepen, A. J.; Da Como, E.; Rogach, A. L.; Feldmann, J. *J. Am. Chem. Soc.* **2010**, *132*, 5981−5983.

(37) Nail, B. A.; Fields, J. M.; Zhao, J.; Wang, J.; Greaney, M. J.; Brutchey, R. L.; Osterloh, F. E. *ACS Nano* **2015**, *9*, 5135−5142.

(38) Yang, Y.; Wang, J.; Zhao, J.; Nail, B. A.; Yuan, X.; Guo, Y.; Osterloh, F. E. *ACS Appl. Mater. Interfaces* **2015**, *7* (10), 5959−5964.

(39) Wang, J.; Zhao, J.; Osterloh, F. E. *Energy Environ. Sci.* **2015**, *8*, 2970−2976.

(40) Zhao, J.; Osterloh, F. E. *J. Phys. Chem. Lett.* **2014**, *5*, 782−786.

(41) Zhao, J.; Nail, B. A.; Holmes, M. A.; Osterloh, F. E. *J. Phys. Chem. Lett.* **2016**, *7*, 3335−3340.

(42) Jia, Q.; Iwase, A.; Kudo, A. *Chem. Sci.* **2014**, *5*, 1513−1519.

(43) Wang, J.; Osterloh, F. E. *J. Mater. Chem. A* **2014**, *2*, 9405−9411.

(44) Tan, H. L.; Suyanto, A.; Denko, A. T. D.; Saputera, W. H.; Amal, R.; Osterloh, F. E.; Ng, Y. H. *Particle & Particle Systems Characterization* **2017**, *34*, 1600290.

(45) Gerischer, H. *J. Electrochem. Soc.* **1966**, *113*, 1174−1182.

(46) Würfel, P. *Physics of Solar Cells*; Wiley-VCH: Weinheim, 2005; p 244.

(47) Dittrich, T. *Materials concepts for solar cells*; Imperial College Press: London, 2015; p xxxiii, 516 pages.

(48) Lewis, N. S. *Inorg. Chem.* **2005**, *44*, 6900−6911.

(49) Peter, L. M. Photoelectrochemistry: From Basic Principles to Photocatalysis. In *Photocatalysis: Fundamentals and Perspectives*; The Royal Society of Chemistry, 2016; pp 1−28, Chapter 1.

(50) Ham, Y.; Hisatomi, T.; Goto, Y.; Moriya, Y.; Sakata, Y.; Yamakata, A.; Kubota, J.; Domen, K. *J. Mater. Chem. A* **2016**, *4*, 3027−3033.

(51) Takashi, H.; Tsutomu, M.; Kazunari, D. *Bull. Chem. Soc. Jpn.* **2012**, *85*, 647−655.

(52) Hisatomi, T.; Maeda, K.; Takanabe, K.; Kubota, J.; Domen, K. *J. Phys. Chem. C* **2009**, *113*, 21458−21466.

(53) Park, H. S.; Leonard, K. C.; Bard, A. J. *J. Phys. Chem. C* **2013**, *117*, 12093−12102.

DOI: 10.1021/acs.nanolett.7b04020
Nano Lett. 2018, 18, 805−810

(54) Zhong, D. K.; Choi, S.; Gamelin, D. R. *J. Am. Chem. Soc.* **2011**, *133*, 18370−18377.
(55) Trzesniewski, B. J.; Digdaya, I. A.; Nagaki, T.; Ravishankar, S.; Herraiz-Cardona, I.; Vermaas, D. A.; Longo, A.; Gimenez, S.; Smith, W. A. *Energy Environ. Sci.* **2017**, *10*, 1517−1529.
(56) Zachäus, C.; Abdi, F. F.; Peter, L. M.; van de Krol, R. *Chemical Science* **2017**, *8*, 3712−3719.
(57) Park, Y.; McDonald, K. J.; Choi, K. S. *Chem. Soc. Rev.* **2013**, *42*, 2321−2337.
(58) Klahr, B.; Gimenez, S.; Fabregat-Santiago, F.; Hamann, T.; Bisquert, J. *J. Am. Chem. Soc.* **2012**, *134*, 4294−4302.
(59) Du, C.; Yang, X. G.; Mayer, M. T.; Hoyt, H.; Xie, J.; McMahon, G.; Bischoping, G.; Wang, D. W. *Angew. Chem., Int. Ed.* **2013**, *52*, 12692−12695.
(60) Sivula, K.; Le Formal, F.; Gratzel, M. *ChemSusChem* **2011**, *4*, 432−449.

DOI: 10.1021/acs.nanolett.7b04020
Nano Lett. 2018, 18, 805−810